Research Article

Molecular Cancer Therapeutics

Inhibition of Tumor Angiogenesis by the Matrix Metalloproteinase–Activated Anthrax Lethal Toxin in an Orthotopic Model of Anaplastic Thyroid Carcinoma

Randall W. Alfano[1,3], Stephen H. Leppla[4], Shihui Liu[4], Thomas H. Bugge[5], Janelle M. Ortiz[3], Terry C. Lairmore[2], Nicholas S. Duesbery[6], Ian C. Mitchell[7], Fiemu Nwariaku[8], and Arthur E. Frankel[1,3]

Abstract

Patients with anaplastic thyroid carcinoma (ATC) typically succumb to their disease months after diagnosis despite aggressive therapy. A large percentage of ATCs have been shown to harbor the V600E B-Raf point mutation, leading to the constitutive activation of the mitogen-activated protein kinase pathway. ATC invasion, metastasis, and angiogenesis are in part dependent on the gelatinase class of matrix metalloproteinases (MMP). The explicit targeting of these two tumor markers may provide a novel therapeutic strategy for the treatment of ATC. The MMP-activated anthrax lethal toxin (LeTx), a novel recombinant protein toxin combination, shows potent mitogen-activated protein kinase pathway inhibition in gelatinase-expressing V600E B-Raf tumor cells *in vitro*. However, preliminary *in vivo* studies showed that the MMP-activated LeTx also exhibited dramatic antitumor activity against xenografts that did not show significant antiproliferative responses to the LeTx *in vitro*. Here, we show that the MMP-activated LeTx inhibits orthotopic ATC xenograft progression in both toxin-sensitive and toxin-resistant ATC cells via reduced endothelial cell recruitment and subsequent tumor vascularization. This in turn translates to an improved long-term survival that is comparable with that produced by the multikinase inhibitor sorafenib. Our results also indicate that therapy with the MMP-activated LeTx is extremely effective against advanced tumors with well-established vascular networks. Taken together, these results suggest that the MMP-activated LeTx-mediated endothelial cell targeting is the primary *in vivo* antitumor mechanism of this novel toxin. Therefore, the MMP-activated LeTx could be used not only in the clinical management of V600E B-Raf ATC but potentially in any solid tumor. *Mol Cancer Ther; 9(1); 190–201. ©2010 AACR.*

Introduction

Anaplastic thyroid carcinoma (ATC) is a highly aggressive disease with only palliative treatments currently available (1). It is thought that a significant portion of these tumors arise from papillary thyroid carcinomas (PTC) that harbor a specific point mutation in the *B-RAF* gene that encodes a kinase component of the mitogen-activated protein kinase (MAPK) pathway (2). A valine to glutamic acid substitution at amino acid position 600 mimics phosphorylation of both Thr^{599} and Ser^{602} residues, resulting in a constitutively active B-Raf kinase that continuously drives downstream effectors independent of upstream growth factor signaling (3, 4). The presence of this V600E B-Raf mutation sensitizes tumor cells to MAPK inhibition so that inhibition of this pathway results in cell cycle arrest and apoptosis (5).

The gelatinase class of matrix metalloproteinases (MMP), consisting of MMP-2 and MMP-9, has been implicated in ATC and PTC invasion, metastasis, and tumor-mediated angiogenesis (6). Expression of these extracellular matrix–degrading enzymes correlates positively with the presence of metastasis and disease progression in thyroid cancer patients (6). The explicit targeting of the V600E B-Raf–mediated MAPK pathway activation in tumor cells with elevated gelatinase expression may provide a novel therapeutic strategy for the clinical management of ATC/PTC.

Anthrax lethal toxin (LeTx) is a binary toxin that consists of protective antigen (PA) and lethal factor (LF). PA is a binding moiety that binds cell surface receptors capillary morphogenesis gene 2 and tumor endothelial marker 8 and translocates LF into cells (7). After binding

Authors' Affiliations: [1]Cancer Research Institute and [2]Department of Surgical Oncology, Scott and White Memorial Hospital; [3]Department of Internal Medicine, Texas A&M Health Science Center, Temple, Texas; [4]Laboratory of Bacterial Diseases, National Institute of Allergy and Infectious Diseases and [5]Oral and Pharyngeal Cancer Branch, National Institute of Dental and Craniofacial Research, NIH, Bethesda, Maryland; [6]Laboratory of Cancer and Developmental Cell Biology, Van Andel Research Institute, Grand Rapids, Michigan; and [7]Division of Gastrointestinal and Endocrine Surgery, Department of Surgery and [8]Department of Surgery, University of Texas Southwestern Medical Center, Dallas, Texas

Note: Supplementary material for this article is available at Molecular Cancer Therapeutics Online (http://mct.aacrjournals.org/).

Corresponding Author: Arthur E. Frankel, Cancer Research Institute, Scott and White Memorial Hospital, 5701 South Airport Road, Temple, TX 76502. Phone: 254-724-0094; Fax: 254-724-2324. E-mail: afrankel@swmail.sw.org

doi: 10.1158/1535-7163.MCT-09-0694

to cell surface receptors, PA is proteolytically activated by furin, which is necessary for subsequent PA heptamerization and binding of up to three LF molecules. The PA/LF complex then migrates into lipid rafts where internalization occurs (8). Progressive acidification of the early endosome induces PA heptamer pore formation and successive LF escape into the cytosol (9). The proteolytic activity of LF causes cleavage and inactivation of all MAP/extracellular signal-regulated kinase (ERK) kinases (MEK), with the exception of MEK5, and thus the inhibition of the ERK1/2, p38, and c-Jun NH_2-terminal kinase branches of the MAPK pathway (10, 11).

Because increased MAPK signaling has been noted in tumors, LeTx has been tested as a potential therapeutic for a variety of tumors (12–17). To improve the specificity of PA for tumor cells, Liu et al. (18) modified the PA furin cleavage site so that it can be cleaved by MMPs. This modified PA, designated PA-L1, is dependent on proteolytic activation by cell surface–bound MMP-2/MMP-9. This MMP-activated LeTx is currently under development for cancer therapy (19, 20).

The selective cytotoxicity of PA-L1/LF has previously been shown in that cell cycle arrest and apoptosis were solely found to occur in human melanoma cells that harbored the V600E B-Raf mutation as well as having high MMP-2/MMP-9 activity *in vitro* (20). However, preliminary *in vivo* studies found that PA-L1/LF treatment exhibited dramatic antitumor activity against xenografts that failed to show an antiproliferative response *in vitro* (21). Further investigation into these preliminary studies determined that PA-L1/LF significantly impairs microvascular endothelial cell invasion and migration in the absence of endothelial cell death (21, 22).

Using an orthotopic model of ATC, we show that PA-L1/LF inhibits ATC progression in both toxin-sensitive and toxin-resistant ATC cells via reduced endothelial cell recruitment and subsequent tumor vascularization. This angiogenesis inhibition translates to an improved long-term survival in tumor-bearing mice that is comparable with that achieved by sorafenib, a multikinase inhibitor currently under evaluation for clinical use in advanced and poorly differentiated PTC (23). In addition, our results indicate that the PA-L1/LF–mediated endothelial cell targeting is extremely effective against advanced tumors with well-established vascular networks. Taken together, these results suggest that the antiangiogenic activity of PA-L1/LF is the primary *in vivo* mechanism and could therefore potentially show activity against any solid tumor.

Materials and Methods

Animals

Male athymic nude mice (NCr-*nu/nu*) 6 to 8 wk of age weighing ≥25 g were purchased from the National Cancer Institute (Frederick, MD) and housed in a pathogen-free environment. Irradiated food and autoclaved water were provided *ad libitum*. Animals were allowed to adjust to their new environment for 1 wk before the initiation of experiments.

Cell Culture

The ATC cell line BHT-101 was purchased from the Deutsche Sammlung von Mikroorganismen und Zelkulturen GmbH. The cell line DRO was generated in the laboratory of Dr. G.F.J. Julliard (University of California, Los Angeles, CA). Cells were cultured in DMEM supplemented with 10% fetal bovine serum and 1% penicillin/streptomycin (Invitrogen) and maintained at 37°C in a 5% CO_2 environment. Experiments were conducted on cells between passages 4 and 8. All cultures were free of *Mycoplasma* species.

Reagents

PA, PA-L1, LF, and LF-β-Lac were produced as previously described (18, 24). The recombinant LF used in this study has the NH_2-terminal sequences HMAGG (25). The fusion protein LF-β-Lac consists of the PA binding domain of LF genetically fused to *Escherichia coli* β-lactamase (24). Sorafenib (Nexavar) was obtained from the Oncology Pharmacy of Scott and White Memorial Hospital. Dilutions for *in vitro* and *in vivo* experiments were done as described previously (26).

Cytotoxicity Assay

BHT-101 or DRO cells were resuspended in complete growth medium at a density of 8×10^4/mL. One hundred microliters were plated per well in Costar 96-well flat-bottomed plates. Cells were allowed to recover, and the medium was exchanged for complete growth medium with or without 5.5 nmol/L LF at final concentration. Serial 3-fold dilutions of PA or PA-L1 at final concentrations of 0 to 10,000 pmol/L or 1.5-fold serially diluted sorafenib at final concentrations of 0 to 60 μmol/L were added, and cells were incubated for 48 h at 37°C/5% CO_2. [^{3}H]Thymidine (1 μCi; NEN DuPont) in 50 μL of complete medium per well was added and incubated at 37°C/5% CO_2 for an additional 18 h. Assays were developed and data were analyzed as described previously (15).

LF Internalization Flow Cytometry

Two hundred and fifty thousand BHT-101 or DRO cells were plated per well in Costar 12-well plates. Cells were allowed to adhere to the plate at 37°C/5% CO_2 and washed once, and fresh AIMV serum-free medium (Invitrogen) was added. Cells were then incubated overnight at 37°C/5% CO_2. LF-β-Lac (90 nmol/L) alone or in combination with 26 nmol/L PA or PA-L1 was added to the conditioned medium and incubated for 5 h at 37°C/5% CO_2. Assays were developed as described previously (20).

Western Blot

Western blots were done as described previously (22). For MEK1 and MEK2 cleavage, BHT-101 and DRO cells were treated with DMSO vehicle, 10 μmol/L sorafenib, and 5.5 nmol/L LF alone or in combination with

10 nmol/L PA/PA-L1 for 16 h in complete growth medium. For phospho-ERK1/2, tumor cells were serum starved for 8 h and then pretreated with inhibitors or toxins in serum-free medium for 16 h. Recombinant epidermal growth factor (EGF; Invitrogen) at 30 ng/mL was added, and cells were incubated for 15 min at 37°C in a 5% CO_2 environment. The rabbit anti-MEK1 (1:500; Millipore), anti-MEK2 (1:500; Santa Cruz Biotechnology), phospho-ERK1/2 (Thr^{202}, Tyr^{204}; 1:250), and total ERK1/2 (1:500; Cell Signaling Technology) antibodies were incubated at 4°C overnight.

PA-L1/LF Efficacy in Orthotopically Implanted ATC Xenografts

All procedures were approved before use by the Institutional Animal Care and Use Committee of Scott and White Hospital. Orthotopic tumors were established as previously described (27). Briefly, all mice received 200 μL i.p. injections of the anti-mouse asialo GM1 antibody (Wako Chemical) diluted 1:8 in PBS at days −4 and −2 to reduce natural killer cells (16). At day 0, animals were sedated via the i.p. administration of 30 μL of 100 mg/mL ketamine/100 mg/mL xylazine cocktail. A midline cervical incision was made, and the underlying submandibular glands were laterally retracted. The midline strap muscles were retracted to expose the thyroid gland and the neighboring trachea. Five hundred thousand BHT-101 or DRO cells in a volume of 5 μL of serum-free DMEM were directly injected into the right thyroid gland using a 25 μL Hamilton syringe fitted with a 30-gauge hypodermic needle, and the skin was closed in a single layer using surgical staples (27). Postoperative i.p. administration of 0.3 mg/mL Buprenex in 1 mL saline was done once daily for 3 d.

Five days after surgery, mice bearing BHT-101 or DRO tumors were randomized and treated with i.p. administration of either 500 μL PBS or 30 μg PA-L1/10 μg LF in 500 μL PBS (five mice per group). Injections were given thrice a week for 2 wk. At day 21, animals were euthanized by i.p. administration of sodium pentobarbital and tumors were removed in continuity with the trachea and larynx as well as the cervical lymph nodes, right submandibular gland, right parotid gland, lungs, and liver. Tumors were measured in all three planes, and the tumor volume was calculated using the formula $V = 4/3(\pi)XYZ$, where X, Y, and Z represent the radius of the tumor in each dimension. Harvested tissues were fixed in 4% neutral-buffered formalin overnight, and H&E staining was subsequently done.

Effects of PA-L1/LF and Sorafenib on the Long-term Survival in Nude Mice Bearing ATC Xenografts

Orthotopic tumor xenografts were established as described above. At day 5, mice bearing BHT-101 and DRO tumors were randomized and treated with i.p. administration of either 500 μL PBS, 30 μg PA-L1/10 μg LF in 500 μL PBS (10 mice per group), 250 μL of 60 mg/kg sorafenib, or vehicle alone via oral gavage (7 mice per group). PA-L1/LF injections were conducted thrice per week for 2 wk, whereas sorafenib was administered daily for 30 d. After the conclusion of treatment regimens, animals were monitored for weight loss, activity level, and appetite and weighed twice weekly. Any animal that became moribund (lethargy, severe weight loss >20%, dehydration, anorexia, hunched posture, etc.) was sacrificed. Experiments were conducted for 55 d.

PA-L1/LF Treatment of Nude Mice Bearing Well-Established ATC Xenografts

Orthotopic tumor xenografts were established as described above. BHT-101 and DRO tumors were allowed to grow for 22 d, and mice were subsequently randomized. Mice received one, two, or four i.p. injections of 30 μg PA-L1/10 μg LF in 500 μL PBS. Eighteen hours after the last dose, mice were euthanized and tumors were harvested and fixed in 4% neutral-buffered formalin overnight, and H&E staining was subsequently done. Percentage of necrotic tissue was determined by the area of tumor cells exhibiting typical necrotic morphologic changes, such as cytoplasmic swelling and diffuse nuclear condensation with the retention of general cellular configuration (28, 29).

Immunohistochemistry

Fixed tumors were sectioned as previously described (27). Endogenous peroxidases were blocked with blocking reagent (DakoCytomation), and slides were washed with distilled H_2O twice more followed by a 5-min wash with wash buffer [PBS (pH 7.5) with 0.05% (v/v) Triton X-100]. Slides were blocked for 1 h with serum-free protein block (DakoCytomation), and primary antibodies diluted 1:50 in antibody diluent [PBS (pH 7.5) supplemented with 1% bovine serum albumin] to Ki-67 (Abcam) or vascular endothelial growth factor (VEGF; Santa Cruz Biotechnology) were added. Antibodies were incubated overnight at 4°C. Slides were washed thrice for 5 min each with wash buffer and developed using the Envision+ System-HRP (DakoCytomation) according to the manufacturer's instructions. All slides were counterstained with Mayer's hematoxylin and permanently mounted.

For CD31 staining, harvested tumors were snap frozen in liquid nitrogen and stored at −80°C until use. Tumors were embedded in OCT medium (Tissue-Tek), and 10-μm sections were mounted on positively charged SuperFrost slides (Fisher Scientific). Slides were air dried for 30 min at room temperature and subsequently fixed in ice-cold acetone for 10 min. Slides were then washed thrice for 5 min each in PBS (pH 7.5), followed by a 10-min wash with wash buffer, and blocked with serum-free protein block (DakoCytomation) for 1 h at room temperature. Monoclonal rat anti-mouse CD31 (Abcam) diluted 1:50 was incubated overnight at 4°C, washed thrice for 5 min each with wash buffer, and then incubated for 1 h with the Texas red–conjugated goat anti-rat secondary antibody diluted 1:100 (Abcam). After three washes,

slides were counterstained with 300 μg/mL Hoechst stain (Sigma-Aldrich) and permanently mounted.

All slides were analyzed with a BX51 microscope fitted with fluorescence (Olympus). Images were obtained with a DP71 digital camera (Olympus). Five slides per mouse were analyzed. For Ki-67, three random areas were chosen per slide and Ki-67–positive cells divided by total number of cells times 100 was determined. Tumor vascularization was determined by the quantification of CD31-positive vessels per 0.6 mm^2 of tissue. Vessel diameter was quantified with the assistance of the DP71 digital camera software (Olympus).

Statistics

Statistical significance of differences was determined using two-tailed *t* tests with GraphPad Prism software (GraphPad Software). All analyses were done assuming Gaussian populations with a 95% confidence interval.

Results

ATC Cells That Are MAPK Dependent and Exhibit High PA-L1 Activation Are Sensitive to PA-L1/LF *In vitro*

The ATC cell line BHT-101 and the cell line DRO are known to carry the V600E B-Raf mutation (30, 31) Cytotoxicity of PA-L1/LF against these cell lines was measured via [^{3}H]thymidine incorporation inhibition. From our experience in the clinical application of immunotoxins, we have designated sensitive cell lines as those for which PA-L1/LF has an IC_{50} of <100 pmol/L, with <10% of control [^{3}H]thymidine incorporation at 10 nmol/L PA-L1/5.5 nmol/L LF. Based on this standard, BHT-101 cells were extremely sensitive to PA-L1/LF (IC_{50}, 20 pmol/L, with 8.7% [^{3}H]thymidine incorporation at 10 nmol/L PA-L1/5.5 nmol/L LF), whereas the cell line DRO was resistant to PA-L1/LF (IC_{50}, 1,255 pmol/L, with 18.3% [^{3}H]thymidine incorporation at 10 nmol/L PA-L1/5.5 nmol/L LF; Fig. 1A).

BHT-101 cells were also sensitive to PA/LF as they were to PA-L1/LF (IC_{50}, 18 pmol/L, with 9.7% [^{3}H]thymidine incorporation at 10 nmol/L PA/5.5 nmol/L LF; Fig. 1B). In comparison, DRO exhibited an 18.6-fold enhanced resistance to PA/LF (IC_{50}, 334 pmol/L, with 1.5% [^{3}H]thymidine incorporation at 10 nmol/L PA/5.5 nmol/L LF; Fig. 1B).

The preceding results suggest that DRO cells express lower levels of MMPs. Lower levels of MMPs may cause decreased PA-L1 activation, reduced LF internalization, and incomplete MAPK inhibition. To test this, we determined the extent of PA-L1 activation in both BHT-101 and DRO cells using the LF variant LF-β-Lac. BHT-101 cells treated with 26 nmol/L of PA or PA-L1 in combination with 90 nmol/L LF-β-Lac were 72% and 97% positive for intracellular LF-β-Lac activity, respectively (Fig. 2A). DRO cells treated with 26 nmol/L PA/90 nmol/L LF-β-Lac were ≥98% positive for intracellular LF-β-Lac activity, whereas cells treated with PA-L1/LF-β-Lac were not significantly different from cells treated with LF-β-Lac alone (Fig. 2A). These results indicate that DRO cells are deficient in their ability to activate PA-L1.

MEK1 and MEK2 cleavage and ERK1/2 phosphorylation in response to EGF in each cell line after PA-L1/LF treatment were tested. Treatment with 10 μmol/L sorafenib, an inhibitor of B-Raf kinase activity, was included as a positive control for ERK1/2 inhibition. BHT-101 cells treated for 16 hours with 10 nmol/L of PA or PA-L1 in combination with 5.5 nmol/L LF exhibited extensive MEK1 and MEK2 cleavage. MEK1 signal was decreased by ≥75% and 74%, whereas MEK2 was decreased by ≥95% and 96% by PA or PA-L1/LF, respectively (Fig. 2B). DRO cells exhibited virtually complete MEK1/2 cleavage when treated with PA/LF, whereas PA-L1/LF treatment induced a 57% and 32% reduction in MEK1 and MEK2, respectively (Fig. 2B). As expected, sorafenib treatment did not reduce total MEK1/2 levels (Fig. 2B).

The decrease in levels of immunoreactive MEK1/2 seen in BHT-101 cells treated with PA or PA-L1 in combination with LF resulted in the complete inhibition of EGF-mediated ERK1/2 phosphorylation (Fig. 2C). As expected, B-Raf kinase inhibition by 10 μmol/L sorafenib reduced ERK1/2 phosphorylation by ≥99% (Fig. 2C). However, the incomplete MEK cleavage in PA-L1/LF–treated DRO cells resulted in the presence of 75% residual ERK1/2 activation in response to 30 ng/mL EGF (Fig. 2C). A complete ERK1/2 inhibition was observed with 10 nmol/L PA/5.5 nmol/L LF, whereas 10 μmol/L sorafenib induced only a 27% decreased phosphorylation (Fig. 2C). Thus, DRO does not activate PA-L1 and therefore does not internalize sufficient amounts of LF for complete MEK1/2 cleavage and consequential ERK1/2 inhibition. Further, DRO does not exhibit appreciable sensitivity to LF-mediated MAPK inhibition, as indicated by its resistance to PA/LF.

PA-L1/LF Treatment Inhibits ATC Tumor Growth *In vivo* via the Inhibition of Tumor Vascularization

BHT-101 or DRO cells were orthotopically implanted into the right thyroid gland of male athymic nude mice. Tumors were allowed to develop and were then treated with PA-L1/LF or PBS. At day 21, mice were euthanized and tumor volume was determined. Mice bearing BHT-101 tumors treated with PBS were found to have a mean tumor volume of 285 mm^3, whereas mice treated with PA-L1/LF were found to have a significant ≥75-fold lower mean tumor volume of 3.7 mm^3 ($P = 0.003$; Fig. 3A). Mice bearing DRO tumors were found to have a similar response to PA-L1/LF treatment. The mean volume of PBS-treated DRO tumors was 200 mm^3, significantly higher than PA-L1/LF–treated DRO tumors with a mean volume of 4 mm^3 ($P = 0.0001$; Fig. 3A).

At the time of necropsy, PBS-treated BHT-101 and DRO tumors were found to be highly vascularized, intricately involved with the neighboring larynx/trachea, and

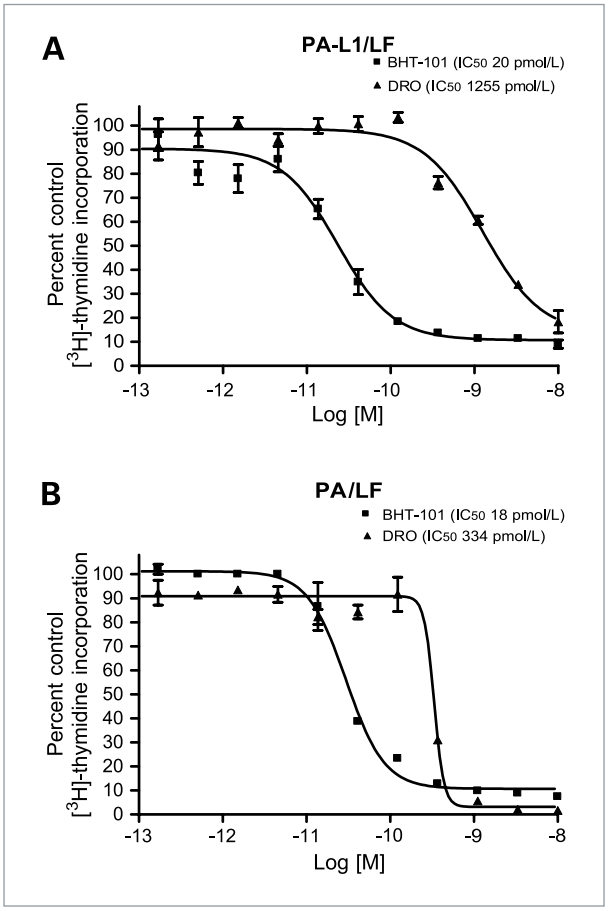

Figure 1. PA-L1 and PA/LF sensitivity of BHT-101 and DRO cell lines. The ATC cell line BHT-101 and the cell line DRO were treated with serial dilutions of PA-L1 or PA, keeping LF at a concentration of 5.5 nmol/L, and the incorporation of [^{3}H]thymidine was measured after 48 h. Data are expressed as a percent of the untreated cell [^{3}H]thymidine incorporation. Sensitivity was arbitrarily set at an IC_{50} of <100 pmol/L, with <10% of control [^{3}H]thymidine incorporation at 10 nmol/L PA-L1/PA in combination with 5.5 nmol/L LF. **A,** BHT-101 (■) was extremely sensitive to PA-L1/LF (IC_{50}, 20 pmol/L, with 8.7% [^{3}H]thymidine incorporation at 10 nmol/L PA-L1/5.5 nmol/L LF), whereas the cell line DRO (▲) was relatively resistant to PA-L1/LF (IC_{50}, 1,255 pmol/L, with 18.3% [^{3}H]thymidine incorporation at 10 nmol/L PA-L1/5.5 nmol/L LF). **B,** the PA-L1/LF–sensitive BHT-101 (■) was also sensitive to PA/LF (IC_{50}, 18 pmol/L, with 9.7% [^{3}H]thymidine incorporation at 10 nmol/L PA/5.5 nmol/L LF). In comparison, DRO (▲) exhibited an 18.6-fold enhanced resistance to PA/LF (IC_{50}, 334 pmol/L, with 1.5% [^{3}H]thymidine incorporation at 10 nmol/L PA/5.5 nmol/L LF).

accompanied by tracheal/esophageal compression. Mice representing each tumor type and treatment group are shown in Fig. 3B. H&E staining showed widespread interdigitation of tumor cells between the thyroid follicles in PBS-treated mice (Supplementary Fig. S1A). The superficial margins of PBS-treated mice showed extensive tumor cell invasion into the strap muscles (Supplementary Fig. S1B). However, no metastatic cells were detected via PCR amplification of the human *β-globin* gene in the cervical lymph nodes, submandibular glands, parotid glands, lungs, or liver (data not shown).

In comparison, BHT-101 and DRO tumors treated with PA-L1/LF exhibited considerable delay in tumor progression. H&E staining showed the presence of tumor cells between the thyroid follicles as seen in PBS-treated mice (Supplementary Fig. S1A). However, the superficial margins were very well defined with minimal tumor cell invasion into the neighboring strap muscles (Supplementary Fig. S1B). The majority of cells in PA-L1/LF–treated tumors were viable, as H&E staining of PA-L1/LF–treated tumors failed to detect tumor cell necrosis. Similarly, terminal deoxynucleotidyl transferase–mediated dUTP nick end labeling (TUNEL) staining did not detect significant apoptosis in these cells (data not shown). These results indicate that PA-L1/LF–mediated inhibition of ATC tumor growth and progression are not associated with increased tumor cell death.

Subsequent analysis of tumor cell cycle progression via the immunohistochemical detection of the Ki-67 antigen determined a significant decrease in BHT-101 and DRO proliferation. PBS-treated BHT-101 tumors were found to consist of ~40% Ki-67–positive tumor cells that were distributed evenly throughout the tumor parenchyma, although these cells exhibited weak staining. BHT-101 tumors treated with PA-L1/LF were reduced to 21% ($P = 0.0001$; Fig. 4A). However, cells of PA-L1/LF–treated xenografts that were positive for Ki-67 exhibited an increase in staining intensity and were found to be on the periphery of the tumor (Fig. 4B). Similarly, DRO cells of PBS-treated tumors were 57% Ki-67 positive, exhibited strong staining, and distributed throughout the tumor parenchyma (Fig. 4B). Treatment with PA-L1/LF was found to reduce Ki-67 staining to 19% ($P = 0.0001$; Fig. 4A). Like BHT-101 xenografts, Ki-67–positive DRO cells in PA-L1/LF–treated xenografts were found on the periphery of the tumor (Fig. 4B). PA-L1/LF treatment did not have an effect on VEGF expression in either BHT-101 or DRO cells (data not shown).

These findings prompted us to determine the extent of tumor vascularization via the quantification of CD31 staining. We found that PBS-treated BHT-101 and DRO tumors exhibited an average of 35.2 and 27.1 vessels per field of view (0.6 mm^2), respectively (Fig. 4C). Vessels of PBS-treated BHT-101 and DRO xenografts were long, tortuous, and disorganized in nature (Fig. 4D). Further, vessels exhibited well-defined lumens (Fig. 4D, *inset*). In contrast, PA-L1/LF–treated xenografts exhibited poor tumor neovascularization. PA-L1/LF–treated BHT-101 tumors contained 83.8% less vessels, with an average of 5.7 vessels per field in tumors ($P < 0.0001$; Fig. 4C). Similarly, PA-L1/LF–treated DRO tumors contained 81.2% less vessels, with an average of 5.1 vessels per field ($P < 0.0001$; Fig. 4C). CD31-positive vessels in PA-L1/LF–treated tumors seemed to be short in length (Fig. 4D). These results indicate that PA-L1/LF–mediated inhibition of ATC tumor growth and progression are accompanied by the loss of tumor vascularization.

PA-L1/LF Has Comparable Effects on Long-term Survival as That of Sorafenib

To determine the effects of this reduction in tumor vascularization on overall ATC xenograft progression, we determined the long-term survival of mice bearing BHT-101 and DRO orthotopic tumors. All mice receiving PBS alone showed rapid disease progression with symptoms of tracheal/esophageal compression by approximately day 20. No survivors were observed past day 32 in either cell line (Fig. 5A).

In contrast, treatment with PA-L1/LF induced a significant increase in survival in both BHT-101 and DRO tumors ($P = 0.0019$ and $P < 0.0001$ for BHT-101 and DRO, respectively; Fig. 5A). An approximate 10-day delay in onset of symptoms was observed that was accompanied by a 1.59-fold improvement in mean survival from 27.5 to 43.8 days for mice bearing BHT-101 tumors (Fig. 5A). Similar results were found in mice bearing the PA-L1/LF–resistant DRO cells. Mean survival was found to increase 1.52-fold from 23.7 days in PBS-treated DRO tumor mice to 36.1 days. These results are consistent with the hypothesis that the inhibition of tumor vascularization translates to a significant increase in mean survival in mice with orthotopic ATC xenografts.

We then compared this improvement in long-term survival with mice treated with the multikinase inhibitor sorafenib, an agent currently under clinical evaluation for thyroid cancer. Sorafenib was equally cytotoxic to BHT-101 and DRO cells *in vitro* (sorafenib IC_{50}, 9.4 and 9.8 μmol/L, with 0.28% and 0.7% [^{3}H]thymidine incorporation at 60 μmol/L sorafenib for BHT-101 and DRO, respectively; data not shown). Mice bearing 5-day-old BHT-101 and DRO tumors received either 60 mg/kg sorafenib or vehicle alone and were treated daily for 30 days. We observed similar effects on long-term survival as that of PA-L1/LF. Mean survival of vehicle-treated mice with BHT-101 xenografts was 23.6 days, whereas that of DRO xenograft–bearing mice was 24.3 days (Fig. 5B). The daily administration of 60 mg/kg sorafenib improved mean survival by 1.82- and 1.46-fold to 43 and 35.7 days for BHT-101 and DRO xenografts, respectively, with one long-term BHT-101 survivor at 55 days ($P = 0.0002$ and $P = 0.0001$ for BHT-101 and DRO, respectively; Fig. 5B).

Improvements in long-term survival by PA-L1/LF and sorafenib were compared (Fig. 5C). Long-term survival of mice bearing BHT-101 tumors treated with PA-L1/LF was not significantly different from those treated with sorafenib ($P = 0.8830$). Similar results were found in mice with DRO xenografts in that treatment with sorafenib did not show significant improvements in long-term survival over that of PA-L1/LF treatment ($P = 0.7360$).

Effects of PA-L1/LF Treatment in Tumors with Preestablished Vasculature

PA-L1/LF has been shown to delay tumor growth via the inhibition of tumor vascularization. We determined

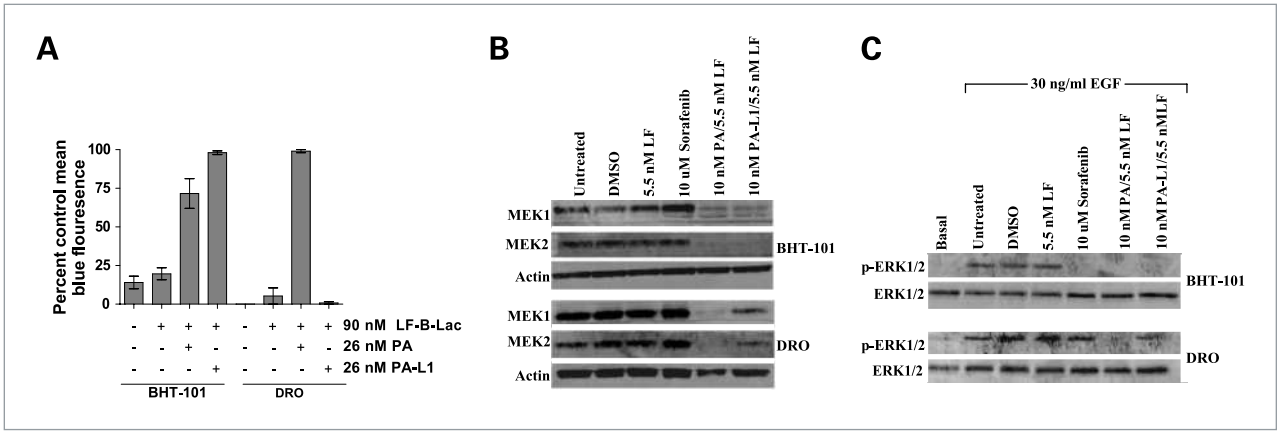

Figure 2. PA-L1 activation, LF internalization, and ERK1/2 inhibition in BHT-101 and DRO cell lines. **A,** BHT-101 and DRO cells were treated with either 90 nmol/L LF-β-Lac alone or in combination with 26 nmol/L PA/PA-L1. Cells were subsequently loaded with the β-lactamase enzyme substrate, the membrane-permeable fluorogenic dye CCF2/AM, and subjected to flow cytometric analysis. Intact CCF2/AM emits fluorescence at 520 nm (*green*) due to intramolecular fluorescence resonance transfer between 7-hydroxycoumarin and fluorescein, whereas LF-β-Lac–mediated CCF2/AM hydrolysis will cause an emission at 447 nm (*blue*) from the liberated donor coumarin. Tumor cell PA/PA-L1 activation and subsequent LF-β-Lac internalization will result in blue light emission, whereas cells that do not internalize LF will emit green fluorescence. *Columns,* mean; *bars,* SE. BHT-101 cells were 72% and 97% positive for blue fluorescence when treated with either 26 nmol/L PA or PA-L1 in combination with 90 nmol/L LF-β-Lac, respectively. PA/LF-β-Lac–treated DRO cells were ≥98% positive for intracellular LF-β-Lac activity, whereas cells treated with PA-L1/LF-β-Lac had negligible blue fluorescence. **B,** PA-mediated and PA-L1/LF–mediated MEK1 and MEK2 cleavage were determined. Treatment of BHT-101 cells with 10 nmol/L PA/PA-L1 in combination with 5.5 nmol/L LF for 16 h exhibited ≥75% and 74% MEK1 cleavage and ≥95% and 96% MEK2 cleavage. DRO cells treated with PA/LF exhibited complete MEK1/2 cleavage, whereas PA-L1/LF treatment induced a 57% and 31.8% reduction in MEK1 and MEK2, respectively. Treatment with 10 μmol/L sorafenib did not reduce total MEK1/2 levels. **C,** pretreated serum-starved BHT-101 and DRO cells were exposed to 30 ng/mL EGF for 15 min to determine ERK1/2 activation levels. The multikinase inhibitor 10 μmol/L sorafenib was included, as phospho–ERK1/2-positive control BHT-101 cells treated with 10 μmol/L sorafenib or 10 nmol/L PA/PA-L1 in combination with 5.5 nmol/L LF reduced ERK1/2 phosphorylation by ≥99%. Sorafenib-treated and PA-L1/LF–treated DRO cells resulted in a modest 27% and 25.1% decrease in ERK1/2 phosphorylation, respectively. Complete ERK1/2 inhibition was observed with 10 nmol/L PA/5.5 nmol/L LF.

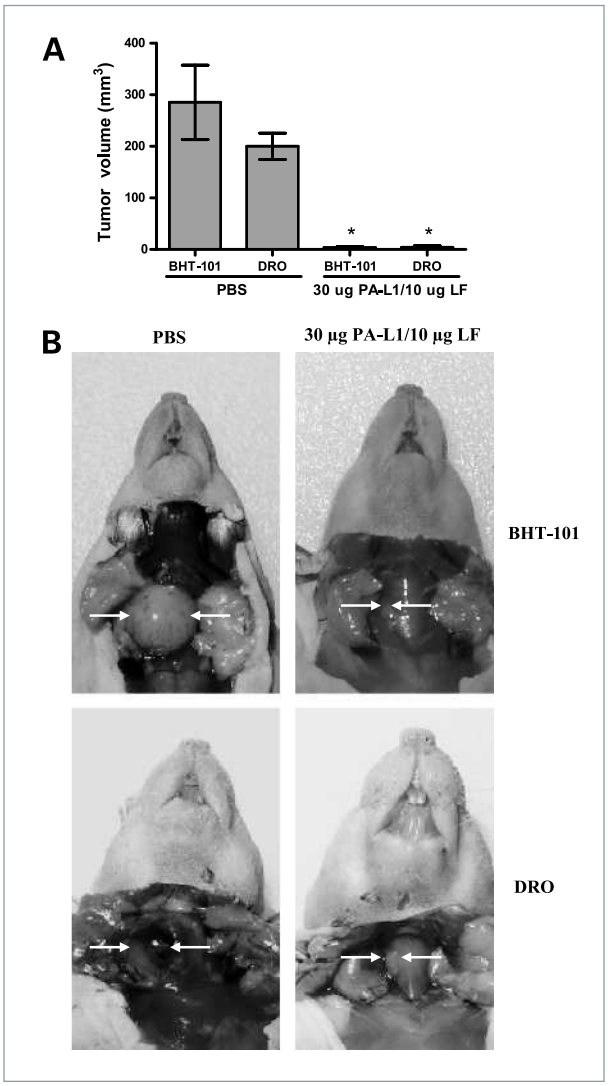

Figure 3. PA-L1/LF efficacy in orthotopic BHT-101 and DRO xenografts. Mice bearing 5-d-old BHT-101 or DRO orthotopic tumors were treated with either 30 µg PA-L1/10 µg LF in 500 µL PBS or PBS alone thrice a week for 2 wk. At day 21, mice were euthanized and tumor volume was determined. *Columns*, mean; *bars*, SE. **A,** PBS-treated BHT-101 and DRO tumors averaged 285 and 200 mm^3, whereas PA-L1/LF–treated tumors were 3.7 and 4 mm^3, respectively. *, $P < 0.05$, unpaired *t* test. **B,** representative mice from each tumor type and treatment group. *White arrows*, tumors.

the effects of PA-L1/LF treatment in tumors with well-established vascular networks. Mice bearing BHT-101 or DRO tumors were randomized at day 22 and treated with one, two, or four doses of 30 µg PA-L1/10 µg LF in 500 µL PBS at days 22, 24, and 26. Eighteen hours after the last scheduled dose, each animal was euthanized and tumor responses were subsequently compared with mice that had not received any intervention. H&E staining revealed that extensive change in tumor cell morphology was consistent with central necrosis appearing 18 hours after the first PA-L1/LF dose in both BHT-101 and DRO tumors (Fig. 6A). BHT-101 tumors exhibited a significant 43.4% increase in necrosis ($P = 0.0013$), whereas DRO tumors showed a significant 41.5% increase ($P < 0.0001$; Fig. 6B). Eighteen hours after the second dose, both BHT-101 and DRO tumors were essentially 100% necrotic and no significant change was observed with four doses of PA-L1/LF (Fig. 6A and B).

A parallel decrease in Ki-67 expression was seen in advanced tumors treated with PA-L1/LF. BHT-101 cells showed a significant 13.9% decrease from 31.0% to 17.1% Ki-67–positive cells ($P < 0.0001$), whereas PA-L1/LF treatment induced a significant 37.9% decrease in DRO cells from 54.8% to 16.9% ($P < 0.0001$; Fig. 6C). Two doses of 30 µg PA-L1/10 µg LF induced essentially 100% cessation of tumor cell proliferation and no significant change with four PA-L1/LF doses. Representative DRO tumors from each dose number are shown in Fig. 6D. To provide a mechanistic understanding of this profound and rapid induction of tumor cell necrosis, we undertook CD31/TUNEL costaining in advanced tumors. However, CD31-positive cells did not colocalize with positive TUNEL staining (Supplementary Fig. S2). Further, no significant difference was detected in CD31 levels between PA-L1/LF–treated and PA-L1/LF–untreated controls (data not shown). Thus, this rapid induction of tumor cell necrosis cannot be attributed to vascular endothelial cell death.

Discussion

Anaplastic thyroid cancer (ATC) is an extremely aggressive malignancy that is associated with rapid progression and death despite conventional chemoradiation therapy (32). Patients who harbor V600E B-Raf–positive PTC/ATC tumors typically present with extrathyroidal invasion, advanced disease, and thus poor clinical prognosis (33). Similarly, the expression of MMP-2/MMP-9 has been shown to correlate with elevated tumor neovascularization, local metastasis, and high clinical stage (6, 34, 35)

These observations validate the preclinical development of PA-L1/LF for V600E B-Raf–positive tumors that exhibit high MMP-2/MMP-9 expression. However, the current study shows that tumor cells, which fail to activate PA-L1 and are resistant to LF-mediated MAPK inhibition *in vitro*, do respond to PA-L1/LF treatment *in vivo*. Both PA-L1/LF–resistant and PA-L1/LF–sensitive tumor types showed a significant reduction in tumor vascularization when PA-L1/LF treatment was initiated early in tumor development. Further, PA-L1/LF treatment proved to be safe as indicated by the absence of significant systemic toxicity. Histologic analysis determined that PA-L1/LF–treated xenografts contained viable tumor cells with a marked absence of necrosis or apoptosis. A similar antiangiogenic effect has been noted in tumors treated with wild-type PA and LF (12, 14). Therefore, these findings show that the inhibition of a nontumor cell compartment such

as endothelial cells, and not direct tumor cell cytotoxicity, is the primary *in vivo* inhibitory mechanism of LF (12, 14, 17, 22).

Comparable results have been obtained with other MAPK targeting agents. PD184352 (CI-1040), a MEK1/2 inhibitor, showed potent tumor growth inhibition in orthotopically implanted V600E B-Raf PTC cells (36). Similarly, BAY 43-9006 (sorafenib), a bi-aryl urea multikinase inhibitor that blocks C-Raf and B-Raf kinase activity, exhibited potent tumor growth inhibition of orthotopic thyroid xenografts (26, 37, 38). Others have reported that sorafenib treatment decreases microvessel density and consequentially induces tumor hypoxia in K1735 murine melanoma xenografts (39).

Several groups have reported the colocalization of TUNEL and CD31 staining in sorafenib-treated subcutaneous and orthotopic xenografts in multiple tumor models (26, 38–40). It is important to note that sorafenib has been reported to inhibit multiple cell surface receptors, including VEGF receptor-2, VEGF receptor-3, platelet-derived growth factor receptor β, Flt-3, and c-Kit (41). Thus, the overall contribution of ERK signaling inhibition to sorafenib-induced

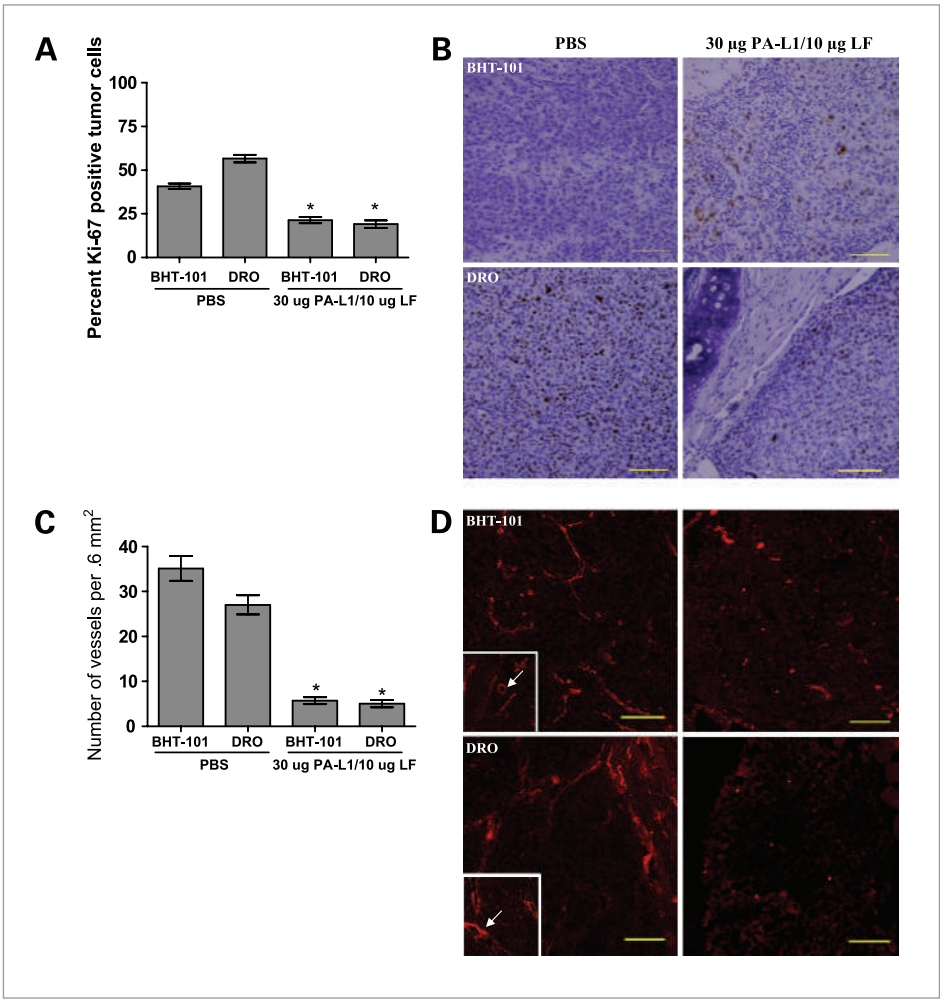

Figure 4. PA-L1/LF inhibits tumor cell proliferation and vascularization. **A,** PBS-treated and PA-L1/LF–treated BHT-101 and DRO tumor cell Ki-67 expression was compared. PBS-treated BHT-101 tumors were found to have 40% tumor cells positive for Ki-67, whereas tumors treated with PA-L1/LF were reduced to 21.4%. PBS-treated DRO tumors were 56.6% Ki-67 positive, whereas PA-L1/LF treatment was found to reduce DRO Ki-67 staining to 19.1%. *Columns,* mean; *bars,* SE. *, $P < 0.05$, unpaired *t* test. **B,** representative Ki-67 immunohistochemical stains from PBS-treated or PA-L1/LF–treated BHT-101 and DRO tumors. PBS-treated tumors showed uniform Ki-67 staining, whereas PA-L1/LF–treated xenografts had Ki-67–positive cells on the periphery of the tumor mass. **C,** tumor vascularization was determined via CD31 staining. PBS-treated BHT-101 and DRO tumors exhibited a mean vascularization of 35.1 and 27.1 vessels per field of view (0.6 mm^2), respectively. PA-L1/LF treatment induced an 83.8% and 81.2% decrease to an average of 5.7 and 5.1 vessels per 0.6 mm^2 in BHT-101 and DRO tumors. *Columns,* mean; *bars,* SE. *, $P < 0.05$, unpaired *t* test. **D,** *inset,* vessels of PBS-treated BHT-101 and DRO xenografts were long, tortuous, and disorganized in nature with observable lumens. In contrast, PA-L1/LF–treated xenografts exhibited poor tumor neovascularization. Vessels that were present were found to be short in length and extremely under developed and had negligible lumen diameters. *Scale bars,* 100 μm. Total magnification, ×100.

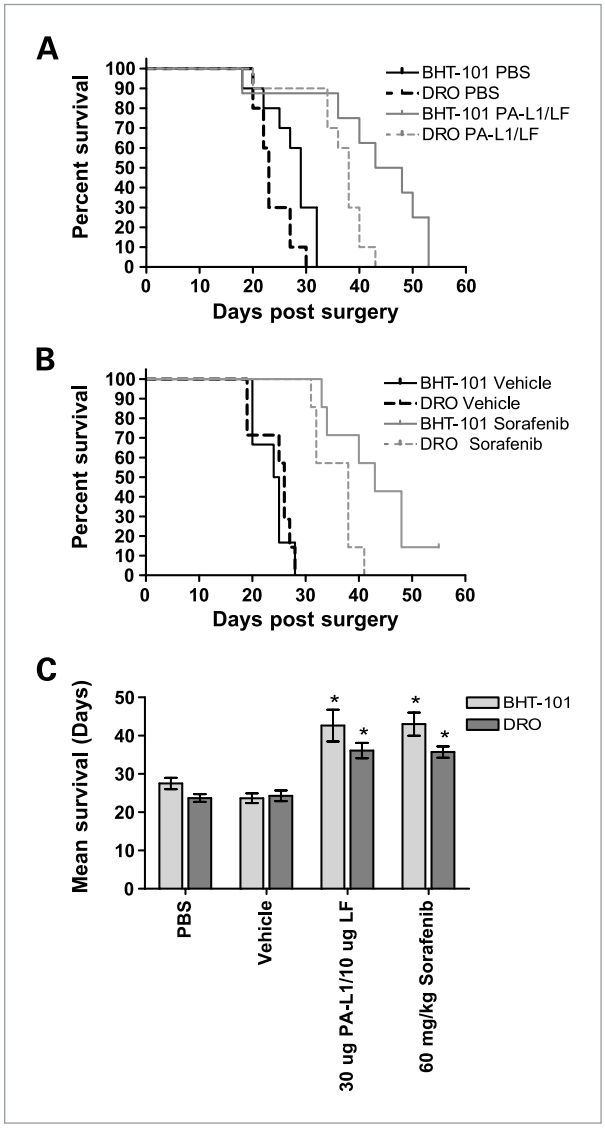

Figure 5. PA-L1/LF treatment significantly improves long-term survival of mice bearing ATC orthotopic xenografts. Long-term survival of mice bearing BHT-101 and DRO orthotopic tumors was determined. **A,** mice bearing BHT-101 (*black solid line*) and DRO (*black dashed line*) receiving PBS alone showed rapid disease progression with no survivors remaining past day 32 in either cell line. PA-L1/LF treatment improved the long-term survival of mice with BHT-101 (*gray solid line*) and DRO (*gray dashed line*) tumors 1.59- and 1.52-fold improvement in mean survival from 27.5 to 43.8 d and 23.7 to 36.1 d, respectively. **B,** mean survival of vehicle-treated mice with BHT-101 (*black solid line*) and DRO (*black dashed line*) xenografts was 23.6 and 24.3 d. Daily therapy with 60 mg/kg sorafenib for 30 d increased mean survival 1.82- and 1.46-fold to 43 and 35.7 d for BHT-101 (*gray solid line*) and DRO (*gray dashed line*) xenografts, respectively. One BHT-101 xenograft mouse treated with sorafenib showed survival to 55 d. **C,** improvements in long-term survival by PA-L1/LF and sorafenib were subsequently compared. Long-term survival of mice bearing BHT-101 (*light gray columns*) and DRO (*dark gray columns*) tumors treated with PA-L1/LF was significantly improved from mice treated with PBS as well as from mice treated with sorafenib versus vehicle alone. However, differences in long-term survival between sorafenib and PA-L1/LF were not significantly different. *Columns,* mean; *bars,* SE. *, $P < 0.05$, unpaired *t* test.

endothelial apoptosis is unknown. Regardless, these findings indicate that MAPK inhibition by LF or by pharmacologic inhibitors primarily blocks tumor growth through inhibition of tumor vascularization (21, 26).

Previously, we have shown that *in vitro* PA-L1/LF treatment of microvascular endothelial cells blocked VEGF-induced endothelial cell MAPK activation (22). MAPK inhibition led to decreased expression of proangiogenic MMPs and reduced the ability of these cells to remodel extracellular matrix proteins collagen type I, collagen type IV, and gelatin (22). PA-L1/LF treatment also reduced endothelial capillary formation *in vitro*, indicating that later steps in the angiogenic remodeling were affected as well (22). Based on these observations, it may be proposed that LF-induced MAPK inhibition has a paralytic-like effect on angiogenic microvascular endothelium that prevents angiogenic remodeling. This in turn causes a temporary inhibition of tumor progression via the reduction of endothelial cell recruitment to the tumor parenchyma and subsequent neovascularization.

According to this hypothesis, PA-L1/LF therapy would be the most effective in early disease, whereas minimal benefit would be expected in tumors with preexisting vasculature. However, both PA-L1/LF–resistant and PA-L1/LF–sensitive xenografts with well-established vascular networks showed significant central necrosis and marked reduction in tumor cell proliferation within 18 hours of a single dose of PA-L1/LF. Previous studies have reported similar results. Ding et al. (17) showed that a single injection of the wild-type LeTx by tail vein injection induced a rapid (24-hour) decrease in tumor perfusion in fibrosarcoma xenografts with well-established vascular networks. Histologic analysis of these LeTx-treated fibrosarcomas determined that significant areas of the tumor contained hemorrhage (17). Additional studies that have addressed vascular barrier function and integrity during systemic anthrax infection further support these findings. The administration of LeTx to mice and nonhuman primates has been shown to induce multiorgan hemorrhage that arises from both large- and small-vessel destruction (42). Assays that quantified this *in vivo* vascular leak determined that LeTx induces extremely rapid vessel dysfunction (42). Thus, it is possible that this observed rapid onset of vascular leak that follows LeTx treatment involves a form of endothelial membrane destabilization (42).

In vitro mechanistic studies involving endothelial monolayers accredited this loss of vascular integrity and ensuing catastrophic vessel dysfunction to the progressive rearrangement of the actin cytoskeleton and altered VE-cadherin distribution in adherens junctions of endothelial cells (43). These junctions, which are critical in endothelial barrier function and monolayer integrity, were seen to change in the course of days and not hours (43). Thus, mechanistic studies have yet to reveal the underlying cause of this rapid loss of tumor perfusion induced by LeTx treatment. However, it is possible that this same

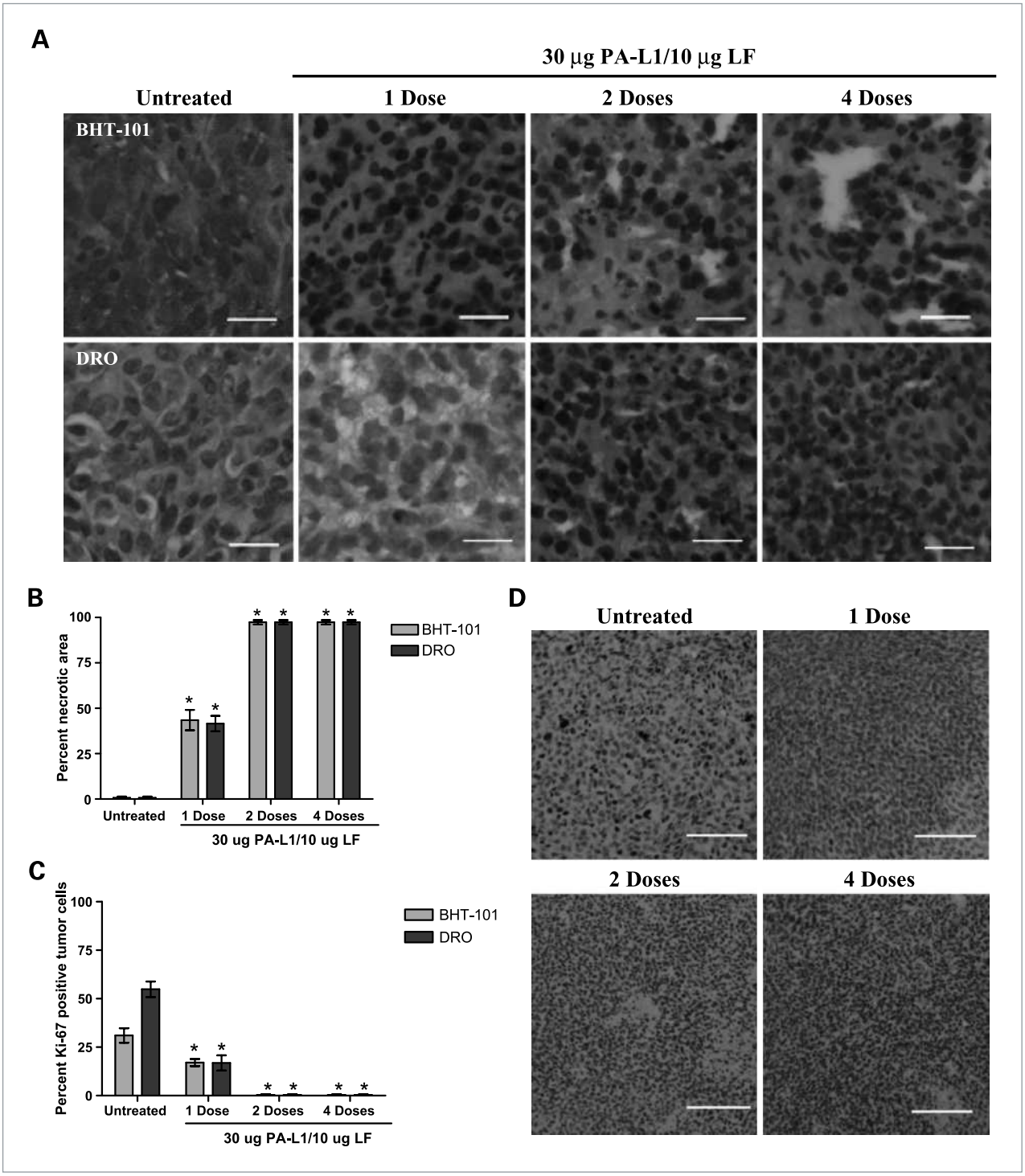

Figure 6. PA-L1/LF treatment exhibits dramatic antitumor activity in late-stage disease. Mice bearing well-established BHT-101 or DRO tumors were treated with either one, two, or four doses of 30 μg PA-L1/10 μg LF. Animals receiving multiple doses were treated every other day. After the last scheduled dose, the animal was euthanized and tumor responses were compared with animals not receiving therapeutic intervention. **A,** H&E staining shows extensive necrosis in both BHT-101 and DRO tumors. *Scale bars,* 20 μm. Total magnification, ×400. **B,** BHT-101 (*light gray columns*) necrosis increased to 43.5% with a single dose of PA-L1/LF, whereas DRO (*dark gray columns*) necrosis increased 41.5%. Both tumors exhibited ≥98% necrotic area with two doses of 30 μg PA-L1/10 μg LF. *Columns,* mean; *bars,* SE. *, $P < 0.05$, unpaired *t* test. **C,** BHT-101 (*light gray columns*) and DRO (*dark gray columns*) tumors exhibited a corresponding 13.9% and 37.9% decrease of Ki-67 expression, respectively. Two doses of 30 μg PA-L1/10 μg LF induced essentially 100% senescence of tumor cell proliferation and no significant change with four PA-L1/LF doses. *Columns,* mean; *bars,* SE. *, $P < 0.05$, unpaired *t* test. **D,** representative DRO tumors from each dose number. *Scale bars,* 100 μm. Total magnification, ×100.

mechanism is responsible for the massive induction of tumor necrosis observed after PA-L1/LF treatment.

In conclusion, our study has shown that the potent orthotopic ATC xenograft growth inhibition showed by PA-L1/LF is derived from toxin action on microvascular endothelial cells. This in turn translates to significant improvements in long-term survival. Further, these results implicate the clinical application of PA-L1/LF in ATC via tumor vasculature targeting.

Disclosure of Potential Conflicts of Interest

No potential conflicts of interest were disclosed.

Acknowledgments

We thank Drs. Josh Combs and Cindy Meininger for helpful discussions and critical reading of the manuscript, Rasem Fattah for assistance with protein purification, and Drs. Rebecca Blackwood and Shu-Ru Kou for technical assistance.

Grant Support

Department of Surgery, Scott and White Memorial Hospital (T.C. Lairmore); Intramural Research Program of the NIH; National Institute of Allergy and Infectious Diseases; and National Institute of Dental and Craniofacial Research.

The costs of publication of this article were defrayed in part by the payment of page charges. This article must therefore be hereby marked *advertisement* in accordance with 18 U.S.C. Section 1734 solely to indicate this fact.

Received 7/30/09; revised 10/26/09; accepted 11/15/09; published OnlineFirst 1/6/10.

References

1. Miccoli P, Materazzi G, Antonelli A, Panicucci E, Frustaci G, Berti P. New trends in the treatment of undifferentiated carcinomas of the thyroid. Langenbecks Arch Surg 2007;392:397–404.
2. Xing M. BRAF mutation in thyroid cancer. Endocr Relat Cancer 2007; 12:245–62.
3. Wan PT, Garnett MJ, Roe SM, et al. Mechanism of activation of the RAF-ERK signaling pathway by oncogenic mutations of B-RAF. Cell 2004;116:855–67.
4. Davies H, Bignell GR, Cox C, et al. Mutations of the BRAF gene in human cancer. Nature 2002;417:949–54.
5. Solit DB, Garraway LA, Pratilas CA, et al. BRAF mutation predicts sensitivity to MEK inhibition. Nature 2006;439:358–62.
6. Maeta H, Ohgi S, Terada T. Protein expression of matrix metalloproteinases 2 and 9 and tissue inhibitors of metalloproteinase 1 and 2 in papillary thyroid carcinomas. Virchows Arch 2001;438:121–8.
7. Young JA, Collier RJ. Anthrax toxin: receptor binding, internalization, pore formation, and translocation. Annu Rev Biochem 2007;76: 243–65.
8. Abrami L, Liu S, Cosson P, Leppla SH, van der Goot FG. Anthrax toxin triggers endocytosis of its receptor via a lipid raft-mediated clathrin-dependent process. J Cell Biol 2003;160:321–8.
9. Puhar A, Monetcucco C. Where and how do anthrax toxins exit endosomes to intoxicate host cells? Trends Microbiol 2007;15: 477–82.
10. Chopra AP, Boone SA, Liang X, Duesbery NS. Anthrax lethal factor proteolysis and inactivation of MAPK kinase. J Biol Chem 2003;278: 9402–6.
11. Duesbery NS, Webb CP, Leppla SH, et al. Proteolytic inactivation of MAP-kinase-kinase by anthrax lethal factor. Science 1998;280:734–7.
12. Duesbery NS, Resau J, Webb CP, et al. Suppression of ras-mediated transformation and inhibition of tumor growth and angiogenesis by anthrax lethal factor, a proteolytic inhibitor of multiple MEK pathways. Proc Natl Acad Sci U S A 2001;98:4089–94.
13. Koo HM, VanBrocklin M, McWilliams MJ, Leppla SH, Duesbery NS, Woude GF. Apoptosis and melanogenesis in human melanoma cells induced by anthrax lethal factor inactivation of mitogen-activated protein kinase kinase. Proc Natl Acad Sci U S A 2002;99:3052–7.
14. Depeille P, Young JJ, Boguslawski EA, et al. Anthrax lethal toxin inhibits growth of and vascular endothelial growth factor release from endothelial cells expressing the human herpes virus 8 viral G protein coupled receptor. Clin Cancer Res 2007;13:5926–34.
15. Abi-Habib RJ, Urieto JO, Liu S, Leppla SH, Duesbery NS, Frankel AE. BRAF status and mitogen-activated protein/extracellular signal-regulated kinase kinase 1/2 activity indicate sensitivity of melanoma cells to anthrax lethal toxin. Mol Cancer Ther 2005;4:1303–10.
16. Abi-Habib RJ, Singh R, Leppla SH, et al. Systemic anthrax lethal toxin therapy produces regressions of subcutaneous human melanoma tumors in athymic nude mice. Clin Cancer Res 2006;12:7437–43.
17. Ding Y, Boguslawski EA, Berghuis BD, et al. Mitogen-activated protein kinase kinase signaling promotes growth and vascularization of fibrosarcoma. Mol Cancer Ther 2008;7:648–58.
18. Liu S, Netzel-Arnett S, Birkedal-Hansen H, Leppla SH. Tumor cell-selective cytotoxicity of matrix metalloproteinase-activated anthrax toxin. Cancer Res 2000;60:6061–7.
19. Alfano RW, Leppla SH, Liu S, Bugge TH, Duesbery NS, Frankel AE. Potent inhibition of tumor angiogenesis by the matrix metalloproteinase-activated anthrax lethal toxin: implications for broad anti-tumor efficacy. Cell Cycle 2008;7:745–9.
20. Alfano RW, Leppla SH, Liu S, et al. Cytotoxicity of the matrix metalloproteinase-activated anthrax lethal toxin is dependent on gelatinase expression and B-RAF status in human melanoma cells. Mol Cancer Ther 2008;7:1218–26.
21. Liu S, Wang H, Currie BM, et al. Matrix metalloproteinase-activated anthrax lethal toxin demonstrates high potency in targeting tumor vasculature. J Biol Chem 2008;283:529–40.
22. Alfano RW, Leppla SH, Liu S, et al. Matrix metalloproteinase-activated anthrax lethal toxin inhibits endothelial invasion and neovasculature formation during *in vitro* morphogenesis. Mol Cancer Res 2009;7:452–61.
23. Kloos RT, Ringel MD, Knopp MV, et al. Phase II trial of sorafenib in metastatic thyroid cancer. J Clin Oncol 2009;27:1675–84.
24. Hobson JP, Liu S, Rono B, Leppla SH, Bugge TH. Imaging specific cell-surface proteolytic activity in single living cells. Nat Methods 2006;3:259–61.
25. Gupta PK, Moayeri M, Crown D, Fattah RJ, Leppla SH. Role of N-terminal amino acids in the potency of anthrax lethal factor. PLoS One 2008;3:e3130.
26. Kim S, Yazici YD, Calzada G, et al. Sorafenib inhibits the angiogenesis and growth of orthotopic anaplastic thyroid carcinoma xenografts in nude mice. Mol Cancer Ther 2007;6:1785–92.
27. Kim S, Park YW, Schiff BA, et al. An orthotopic model of anaplastic thyroid carcinoma in athymic nude mice. Clin Cancer Res 2005;11: 1713–21.
28. Searle J, Lawson TA, Abbott PJ, Harmon B, Kerr JF. An electron-microscope study of the mode of cell death induced by cancer-chemotherapeutic agents in populations of proliferating normal and neoplastic cells. J Pathol 1975;116:129–38.

29. Golstein P, Kroemer G. Cell death by necrosis: towards a molecular definition. Trends Biochem Sci 2007;32:37–43.
30. Nikiforova MN, Kimura ET, Gandhi M, et al. BRAF mutations in thyroid tumors are restricted to papillary carcinomas and anaplastic or poorly differentiated carcinomas arising from papillary carcinomas. J Clin Endocrinol Metab 2003;88:5399–404.
31. Liu D, Liu Z, Jiang D, Dackiw AP, Xing M. Inhibitory effects of the mitogen-activated protein kinase kinase inhibitor CI-1040 on the proliferation and tumor growth of thyroid cancer cells with BRAF or RAS mutations. J Clin Endocrinol Metab 2007;92:4686–95.
32. Chiacchio S, Lorenzoni A, Boni G, Rubello D, Elisei R, Mariani G. Anaplastic thyroid cancer: prevalence, diagnosis and treatment. Minerva Endocrinol 2008;33:341–57.
33. Liu Z, Hou P, Ji M, et al. Highly prevalent genetic alterations in receptor tyrosine kinases and phosphatidylinositol 3-kinase/akt and mitogen-activated protein kinase pathways in anaplastic and follicular thyroid cancers. J Clin Endocrinol Metab 2008;93:3106–16.
34. Buergy D, Weber T, Maurer GD, et al. Urokinase receptor, MMP-1 and MMP-9 are markers to differentiate prognosis, adenoma and carcinoma in thyroid malignancies. Int J Cancer 2009;125:894–901.
35. Komorowski J, Pasieka Z, Jankiewicz-Wika J, Stepień H. Matrix metalloproteinases, tissue inhibitors of matrix metalloproteinases and angiogenic cytokines in peripheral blood of patients with thyroid cancer. Thyroid 2002;12:655–62.
36. Henderson YC, Ahn SH, Clayman GL. Inhibition of the growth of papillary thyroid carcinoma cells by CI-1040. Arch Otolaryngol Head Neck Surg 2009;135:347–54.
37. Awada A, Hendlisz A, Gil T, et al. Phase I safety and pharmacokinetics of BAY 43-9006 administered for 21 days on/7 days off in patients with advanced, refractory solid tumours. Br J Cancer 2005;92:1855–61.
38. Keating GM, Santoro A. Sorafenib: a review of its use in advanced hepatocellular carcinoma. Drugs 2009;69:223–40.
39. Murphy DA, Makonnen S, Lassoued W, Feldman MD, Carter C, Lee WM. Inhibition of tumor endothelial ERK activation, angiogenesis, and tumor growth by sorafenib (BAY43-9006). Am J Pathol 2006; 169:1875–85.
40. Liu L, Cao Y, Zhang X, et al. Sorafenib blocks the RAF/MEK/ERK pathway, inhibits tumor angiogenesis, and induces tumor cell apoptosis in hepatocellular carcinoma model PLC/PRF/5. Cancer Res 2006;66:11851–8.
41. Wilhelm S, Carter C, Tang L, et al. BAY 43-9006 exhibits broad spectrum oral antitumor activity and targets the RAF/MEK/ERK pathway and receptor tyrosine kinases involved in tumor progression and angiogenesis. Cancer Res 2004;64:7099–109.
42. Warfel JM, Stelle AD, D'Agnillo F. Anthrax lethal toxin induces endothelial barrier dysfunction. Am J Pathol 2005;166:1871–81.
43. Gozes Y, Moayeri M, Wiggins JF, Leppla SH. Anthrax lethal toxin induces ketotifen-sensitive intradermal vascular leakage in certain inbred mice. Infect Immun 2006;74:1266–72.